Bulletin of the Mineral Research and Exploration

http://bulletin.mta.gov.tr

Simulation of a salt dome using 2D linear and nonlinear inverse modeling of residual gravity field data

Soheyl POURREZA[a] and Farnush HAJIZADEH[a*]

[a]Faculty of Mining Engineering,Urmia University, Urmia, Iran.

Research Article

Keywords:
Gravity, Inversion, Salt dome, Underdetermined.

ABSTRACT

In gravity field inversion we usually dealing with underdetermined problems and for obtaining realistic solutions can introduce a depth-weighting function to the inversion algorithm. We employ a linear inversion method for determining the underground density distribution of the gravity causative mass. The validation and accuracy of method is tested on two synthetic gravity anomaly from different models, while the data are noise- free and corrupted with noise. In this paper, We also invert the 2D gravity anomaly produced by a salt dome from the northwest of Iran. The salt domes in the region under investigation are a rich source of Potash. The inverted structure demonstrate on average a depth to top and bottom of 27 m and 65 m, respectively. For comparison, we also have simulated the salt dome using the nonlinear inverse modeling. The results are mostly similar.

Received Date: 03.06.2018
Accepted Date: 15.10.2018

1. Introduction

Gravity investigation has been used widely over the years for inverse modeling of various buried geological structures and deposit mass, especially in mineral reconnaissance projects (Mandal et al., 2013; Biswas et al., 2014*a, b*; Mandal et al., 2015; Biswas and Sharma, 2016). The nonuniqueness in the linear inverse problem of gravity, i.e., the existence of a large variety of distribution of undersurface density models that generate a similar gravity effect on measurement plane, hesitate the reliability of solution (Skeels, 1947; Parker, 1973; Biswas, 2015; 2016; Singh and Biswas, 2016; Biswas et al., 2017). In order to obtain the correct unique solution and minimizing the ambiguities, various researchers have been proposed different algorithms to increase the amount of extracted information from inversion for simulating the geometry of a density distribution due to a distinct gravity anomaly, as the proposed model be geologically realistic (Srivastava et al., 2007; Ganguli and Dimri, 2013; Biswas, 2015; Ganguli et al., 2015; Singh and Biswas, 2016; Biswas et al., 2017).

Tsuboi (1983) introduce a simple but effective approach based on equivalent stratum technique to estimate 3D topography of a density interface. Oldenburg (1974) proved that the Parker's expression could be applied in order to specify the geometry of the density distribution from the residual gravity anomaly. The geological maps and petrophysical data from rock samples were used to to approximate the model parameters to realistic values (Farquharson et al., 2008; Williams, 2008; Heincke et al., 2010; Lelièvre et al., 2012; Tschirhart et al., 2013; 2017). Kamm et al. (2015) used the petrophysical information for joint inversion of magnetic and gravity. Moreover, there are uniform and permanent models in the inversion of gravity and magnetic fields and their derivatives (Biswas, 2018; Lalongo et al., 2014).

Using a joint inversion of multiple data sets can also diminish the nonuniqueness of the inverse problem, examples of joint inversion of gravity and magnetic data are given by, e.g., Zeyen and Pous (1993), Gallardo and Meju (2003), and Pilkington (2006) using deterministic inversion techniques

Citation info: Pourreza,S., Hajizadeh, F. 2019. Simulation of a salt dome using 2D linear and nonlinear inverse modeling of residual gravity field data. Bulletin of the Mineral Reserach and Exploration, 160, 231-244. *http://dx.doi.org/10.19111/bulletinofmre.502021*

* *Corresponding author: Farnush HAJIZADEH, f.hajizadeh@urmia.ac.ir*

and by Bosch and McGaughey (2001) and Bosch et al. (2006) using stochastic methods. Shamsipour et al. (2010, 2011, 2012) proposed the cokriging as a geostatistical method and conditional simulation for the discrete 3-D inversion of magnetic and gravity data respectively, including geological restrictions.

One way to eliminate this ambiguity is to put a appropriate geometry shape to the anomalous mass with a known density followed by inversion of gravity anomalies (Chakravarthi and Sundararajan, 2004). Although customary geometry models may not be geologically realistic, they are usually being sufficient to analyze causative mass of many isolated gravity anomalies (Abdelrahman and El-Araby, 1993). The interpretation of such an anomaly aims essentially to compute the parameters such as depth, shape, and radius of the gravity anomaly causative body such as geological structures , mineral mass and artificial underground structures (Singh and Biswas, 2016; Biswas, 2015). Thus, in this case deal with the nonlinear inverse modeling.

Several graphical and numerical methods have been developed for analyzing residual gravity anomalies caused by simple bodies, such as Saxov and Nygaard (1953) and Bowin et al. (1986). The methods include, for example, Fourier transform (Odegard and Berg, 1965; Sharma and Geldart,1968); Mellin transform (Mohan et al., 1986); Walsh transforms techniques (Shaw and Agarwal, 1990); ratio techniques (Hammer, 1977; Abdelrahman et al., 1989); least-squares minimization approaches (Gupta, 1983; Lines and Treitel, 1984; Abdelrahman, 1990; Abdelrahman et al., 1991), different neural networks (Salem et al., 2001; Osman et al., 2006; 2007; Al-garni, 2013; Eshaghzadeh and kalantari, 2015; Eshaghzadeh and Hajian, 2018); very fast simulated annealing (Biswas et al., 2017; Biswas, 2015; 2016) Particle swarm optimization (Singh and Biswas, 2016); effective quantitative interpretations using the least-squares method (Gupta, 1983) based on the analytical expression of simple moving average residual gravity anomalies are yet to be developed. Abdelrahman and El-Araby (1993) introduced an interpretive technique based on fitting simple models convolved with the same moving average filter as applied to the measured gravity. A simple approach introduced by Essa (2007) is applied to determine the shape factor and depth of simple features from residual gravity anomalies along the profile. Another automatic method, e.g. the least-squares method, was offered by Asfahani and Tlas (2008), by which the depth and amplitude coefficient can be specified.

In this study, we employ the linear inverse modeling technique using depth weighting parameter as resolution enhancer and one-norm (also known as the L1 norm or mean norm) as stopping criteria in inversion algorithms for a real gravity data due to a salt dome in the north of the Zanjan province, Iran. The salt domes situated in the north of the Zanjan province and the south of the East Azerbaijan province are volumetrically small and near the surface. These salt domes are the rich resources of the Potash.

2. Computing the Kernel Matrix

For inverting the gravity data and calculating a 2D density distribution corresponding to the gravity anomaly, it is necessary that the gravity response due to the ground of the sub-surface as has been divided to several prisms be computed at the surface. For a 2-D model, as shown in figure 1, the gravity response of all the rectangular prisms at the observation point *i*, is given by:

$$g_i = \sum_{j=1}^{M} P_{ij} d_j, \quad i = 1,...,N \qquad \text{(equation 1)}$$

where M and N denote the number of blocks and the number of observations, respectively, d_j is the density of the j^{th} block and P_{ij} is matrix of geometric element or kernel matrix which presenting the influence of the j^{th} block on the i^{th} gravity value. In order to calculate the kernel matrix P_{ij}, the gravity response of the 2D prism using equation developed by Last and Kubik (1983) is estimated, as:

$$p_{ij} = 2G \begin{bmatrix} (x_i - x_j + \frac{d}{2}) \log(\frac{r_2 r_3}{r_1 r_4}) + d \log(\frac{r_4}{r_3}) - \\ (z_j + \frac{h}{2})(\theta_4 - \theta_2) + (z_j - \frac{h}{2})(\theta_3 - \theta_1) \end{bmatrix}, \qquad \text{(equation 2)}$$

where;

$$r_1^2 = (z_j - \frac{h}{2})^2 + (x_i - x_j + \frac{d}{2})^2,$$

$$r_2^2 = (z_j + \frac{h}{2})^2 + (x_i - x_j + \frac{d}{2})^2,$$

$$r_3^2 = (z_j - \frac{h}{2})^2 + (x_i - x_j - \frac{d}{2})^2,$$

$$r_4^2 = (z_j + \frac{h}{2})^2 + (x_i - x_j - \frac{d}{2})^2,$$

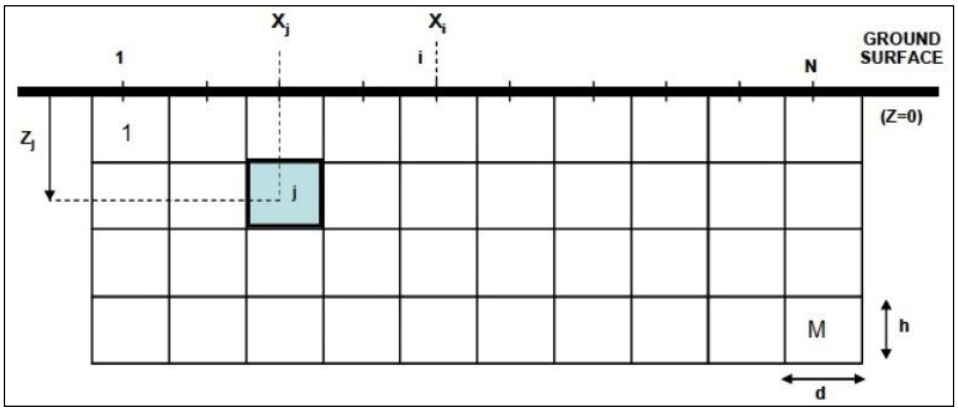

Figure 1- A simple 2D model of the inversion domain as has been divided to several blocks with a dimension of i×j.

and

$$\theta_1 = \tan^{-1}(x_i - x_j + \frac{d}{2}) / (z_j - \frac{h}{2}),$$

$$\theta_2 = \tan^{-1}(x_i - x_j + \frac{d}{2}) / (z_j + \frac{h}{2}),$$

$$\theta_3 = \tan^{-1}(x_i - x_j - \frac{d}{2}) / (z_j - \frac{h}{2}),$$

$$\theta_4 = \tan^{-1}(x_i - x_j - \frac{d}{2}) / (z_j - \frac{h}{2}),$$

Here G is the gravitational constant, d and h are the width and height of the each block.

3. Inversion Method

In most of the inverse modeling cases, we deal with the underdetermined problems, i.e. the number of unknowns is much greater than the number of observed data. For a general underdetermined system of linear equations, i.e. $d=Pf$ where d is the column vector of the observed gravity field data, f is the column vector of the unknown, i.e. density, and P is the kernel rectangular matrix, the minimum norm solution is defined as the model that fits the data exactly which is given by (Menke, 1984):

$$f = P^T (PP^T)^{-1} d, \qquad \text{(equation 3)}$$

The super script T denotes the matrix transposition. This expression usually leads to an unrealistic density distribution. We can solve the inversion problem using the weighted–damped least-squares method, as (Last and Kubik, 1983):

$$f = W_f^{-1} P^T (P W_f^{-1} P^T + W_n^{-1})^{-1} d, \qquad \text{(equation 4)}$$

If assumed that there are M prisms of unknown density (number of model parameters) and N observed gravity data (Figure 1), therefore, f is a $M\times1$ vector of the unknown density and d is a $N\times1$ vector of the observed gravity data. The density weighting matrix (W_f), noise-weighting matrix (W_n) and kernel matrix (P) have also the dimensions $M\times M$, $N\times N$ and $N\times M$, respectively. The density weighting matrix is given by (Last and Kubik, 1983):

$$\left[W_f^{(k-1)}\right]_{ii}^{-1} = \left[f_i^{(k-1)}\right]^2 + \varepsilon, \qquad \text{(equation 5)}$$

where k is the iteration and constants ε is the perturbation number as should be chosen as small as possible without causing numerical inconstancy, generally is assumed about 10^{-10} to 10^{-13}. The noise-weighting matrix is defined at each iteration as:

$$W_n^{-1} = l_0^2 diag(P w_f^{-1} P^T), \qquad \text{(equation 6)}$$

As the l_0 is a priori estimated noise/signal ratio. The weighting functions are specifically designed to minimize the area of the model, that is, to maximize its compactness. After computing the density amount of each block in each iteration, the gravity effect of the blocks whose estimated values are greater than the initial defined amount, must be eliminated. The formulation is (Last and Kubik, 1983):

$$g_i^k = g_i - b\sum_j P_{ij} H\left[f_j^{(k-1)}/b\right], \quad i = 1,...,N, \qquad \text{(equation 7)}$$

where b is being the target density and H denotes the Heaviside step function, as here, whose value is zero for smaller or equal values to one and one for values larger than one,

$$H[n]=\begin{cases}0, & n\le 1\\ 1, & n>1\end{cases} \qquad \text{(equation 8)}$$

It is worth mentioning, the Heaviside step function is used to eliminate the gravity effect of the blocks whose the estimated density are greater than the target density from the gravity data. When the density value of the specific block gets bigger than a interface density (b), the algorithm establishes the density of the block equal to b and automatically separates the block in the next iterative during inversion process. This is achieved by subtracting its gravity effect from the total gravity anomaly and assigning it a very large weight, thus the equation 7, estimate a reduced gravity data vector in each step (Last and Kubik, 1983).

The method consists of an iterative procedure in which the weighting matrices alter at each iteration until an acceptable convergence of the solution is obtained and eventually a compact final model is generated (Last and Kubik, 1983). In inverting gravity data due to a causative mass, the evaluated density distribution related to buried structure tend to concentrate near the surface. For nullifying the natural decay of the kernels and maximizing the depth resolution, a depth weighting function is inset in the problem. Li and Oldenburg (1998) offered to employ a depth weighting function such as:

$$w_z=\frac{1}{(z+z_o)}, \qquad \text{(equation 9)}$$

where z is the depth of the layers and z_0 depends on the cell size of the model and the observation height of the gravity data.

In this paper, we employ the one-norm (*L1* norm) as a criterion for stopping the iteration process in inversion algorithms. The *L1* norm has the form:

$$L1\ \ norm:\quad \|e\|_1=\left[\sum_k |e_k|\right], \qquad \text{(equation 10)}$$

Where the e is the difference between the observed gravity data and inverted gravity data due to the evaluated model from the density distribution at each iteration. As soon as the *L1* norm achieve the lowest amount which usually coincides with minimum area of the density distribution, the iteration is terminated. We can summarize the inversion process as the following algorithm,

Input: *d, P, ε, l_0*

Output: *f*

for i=1:k do

Calculate: W_f, W_n

Compute: *f, L1*

If $L1_{(i-1)}<L1_i$

Break

end

Apply: *Heaviside function*

Compute: *d*

end

4. Synthetic Models

The proficiency and validity of the compact inversion method is illustrated with two set of synthetic gravity data. We assign the ε and l_0 as 10^{-10} and 0.1 respectively, for inverting the theoretical gravity data. Figure 2(a) shows the gravity response to the assumed model in figure 2(b) where the subsurface ground has been partitioned into 15×10 prisms as the dimension of each prism is 10 m × 5 m. As is shown in figure 2b, the 2D model include 12 prisms whose the density contrast is -1000 kg/m^3. The inverted gravity corresponding to the resulted causative body from inverting the observed gravity (Figure 2c), is displayed in figure 2(a). This inverted model that is exactly similar of the original causative body, achieved at 8th iteration, where the L1 norm as the stopping criterion attain the smallest amount. The L1 norm, reduces intensely from its initial value of 0.71 mGal at the first iteration to 0.031 mGal at the end of the 5th iteration and then gradually reaches zero (very close to zero) mGal at the 8th iteration (Figure 6a).

Figure 3(a) shows the computed gravity for the assumed model in figure 3(b) where the subsurface inversion domain has been divided into 25×10 blocks of dimension 4 m × 5 m. Therefore, the whole domain is 100 m × 50 m and the total number of blocks is M=250. considering figure 3b can see that the 2D model include 18 prisms whose the density contrast is -1000 kg/m^3. In recent theoretical model, the inversion domain has been composed of the smaller blocks than the first model. figures 4 (a), 4(b) and 4(c) represent the inferred density distribution from the inversion

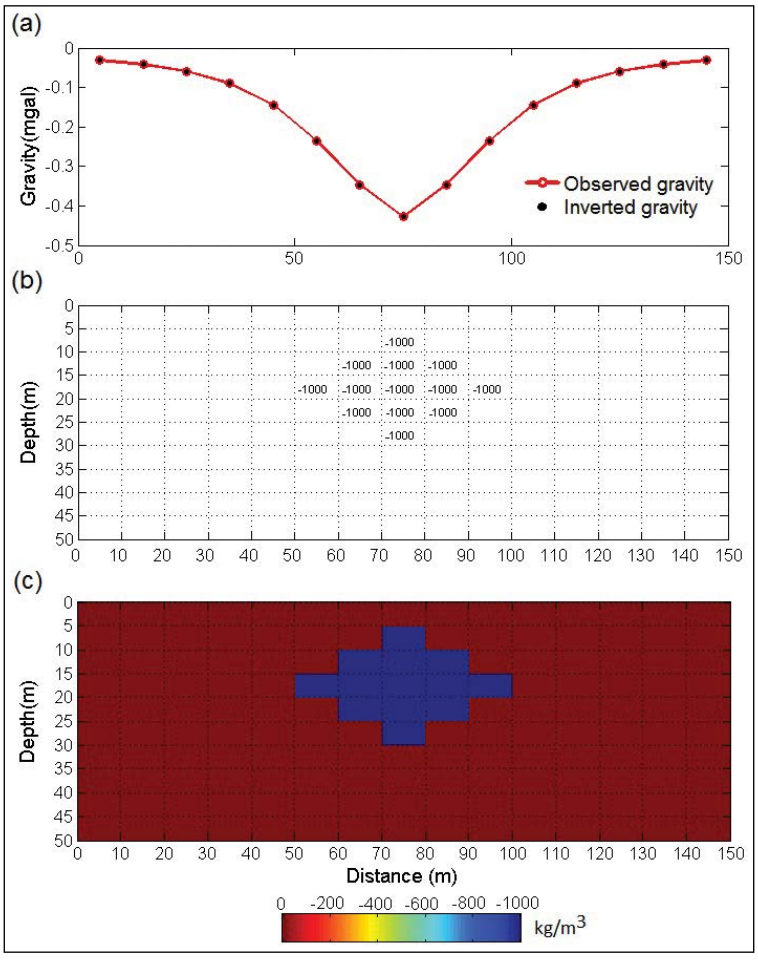

Figure 2- a) Observed and inverted gravity due to b) assumed model and c) inverted model, respectively.

the observed gravity after 3rd, 5th and 7th iterations, respectively. At 7th iteration, L1 norm amount is minimum one. Figure 6(b) exhibit the variations the L1 norm values versus the iteration during inversion for the observed gravity in figure 3(a). With attention to figures 4 can clearly find during inversion process the number of the blocks which are masked with high density decrease. The 3rd iteration produced a spread-out density distribution, but at the 5th iteration the compactness has been increased, as at the 7th iteration the minimum area of the blocks with maximum density, regardless to the sign of density, has been yielded. The inverted gravity due to the resulted model in figure 4(c) is shown in figure 3(a).

The efficiency of the inversion approach in the presence of error is tested after adding 10% random noise to the gravity data in figure 3(a). The noise corrupted synthetic gravity data has been brought in figure 5(a). Figures 5 (b), 5(c) and 5(d) demonstrate the configuration of density distribution between prisms resulted from the inversion the observed gravity data corrupted with noise at 5th, 7th and 9th iterations, respectively. With the iterations proceeding, the area of the interpreted structure is diminishes as at the 7th iteration a fairly compact model is inferred. By the 9th iteration the procedure give a almost converged results to the desired initial model. The L1 norm value decreases gradually from its initial value of 0.727 mGal at the first iteration to 0.078 mGal at the 9th iteration (Figure 6c), where L1 norm amount is minimum. Therefore, the figure 5(d) shows the most similar shape to the assumed causative body by inversion the gravity data corrupted with random noise. The inverted gravity data due to interpreted model in figure 5(d) has been shown in figure 5(a).

We also studied the stability of the inversion technique for the observed gravity data with a higher level of noise, as it corrupted with 15% random noise

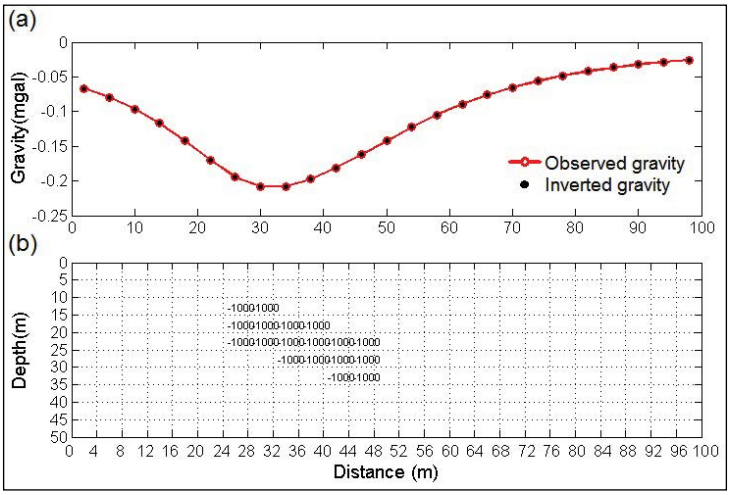

Figure 3- a) observed and inverted gravity b) assumed model

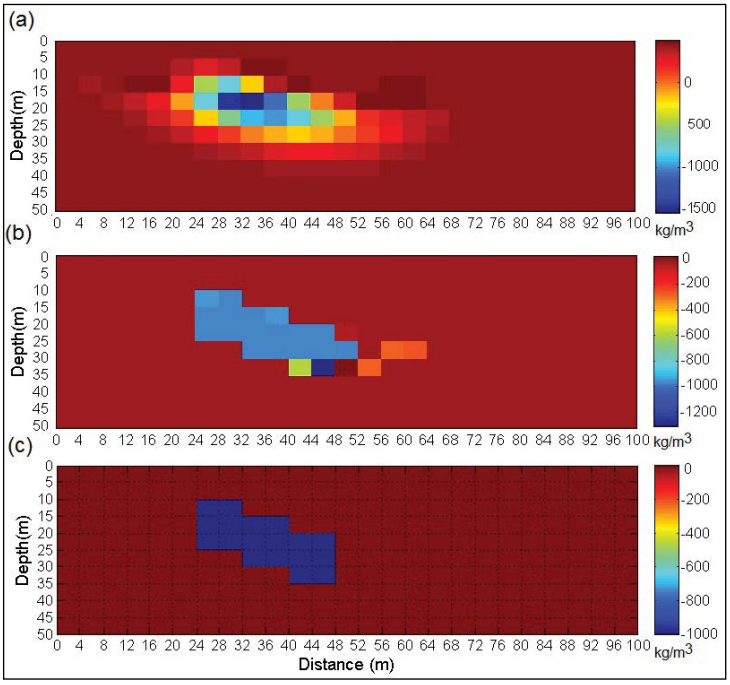

Figure 4- Inverted models at a) 3rd, b) 5th and c) 7th iterations, respectively

(Figure 7a). The interpreted density distribution is shown in figure 7(b) as the buried structure has been specified by the black line. The algorithm stopped at 14th iteration, where the L1 norm became 1.32 mGal. Considering the inferred results prove the validity of the inverse modeling method.

The analysis of the synthetic models, with and without random noise, eventuate the satisfactory results which confirm the performance and stability of the inversion method.

5. Field Example

The region under study is situated in the north of the Zanjan province, the northwest of Iran. Miocene stage in this area are characterized by rapid subsidence, deposition, and facies changes in both marine and continental sedimentary basins as Miocene units in the study region include sequences of Marl, Salt and Chalk. Figure 8 show the geological map of the region under investigation. The gravity measurement region is approximately even morphologically. The height

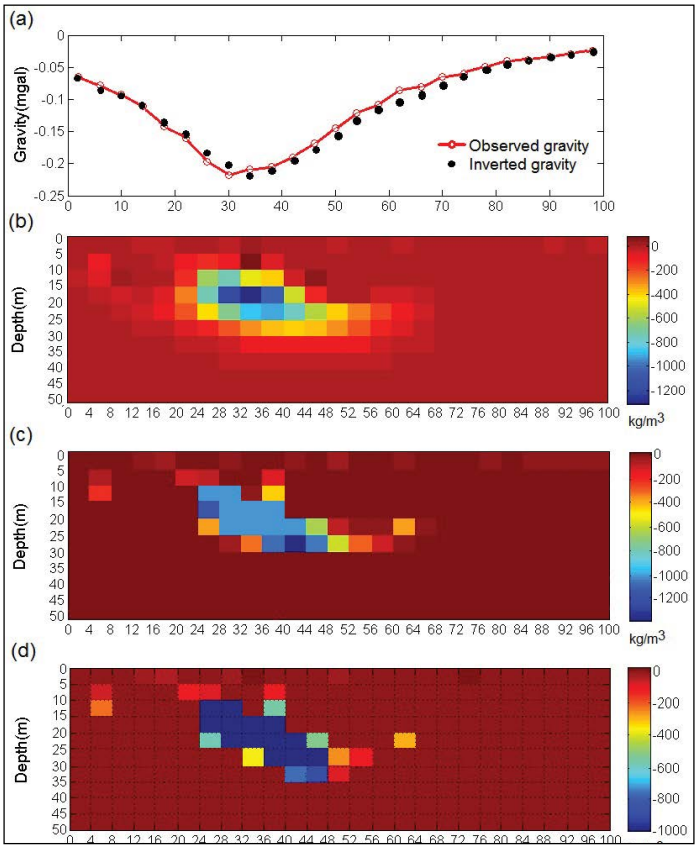

Figure 5- a) Observed gravity due to model in figure 3(b) as corrupted with 10% noise and inverted gravity b) inverted model at 5th iteration, c) inverted model at 7th iteration and d) inverted model at 9th iteration

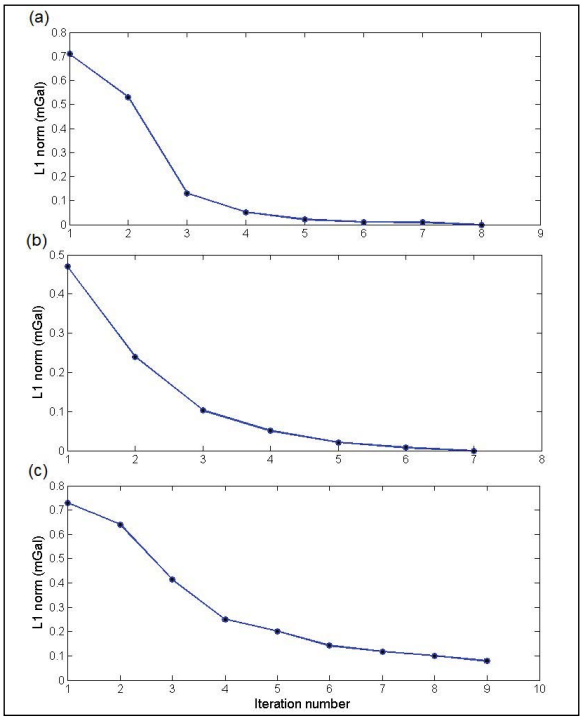

Figure 6- Variations L1 norm values versus iteration number for analyzing a) the observed gravity data in figure 2(a), b) the observed gravity data in figure 3(a), c) the noisy observed gravity data in figure 4(a)

variations the region under evaluation is illustrated in figure 9.

The salt domes in this area are the result of the upward movement of the Neogene evaporative materials as their connection with the mother salt layer have been interrupted (Figure 10). The depth of these salt domes is shallow and their volume is low. These salt dome have mostly high percentage of Potash.

The main salt dome in the region under consideration is Aji-chay salt dome. An area that the gravity studies has been performed, with a white rectangular on figure 8 has been determined. Figure 11 show the computed Bouguer gravity anomaly after making the necessary corrections. The Bouguer gravity anomaly map demonstrate a dominant regional gravity field which increase from south to north. After removing a trend (degree 2) from the Bouguer anomaly, the residual (local) gravity anomalies which

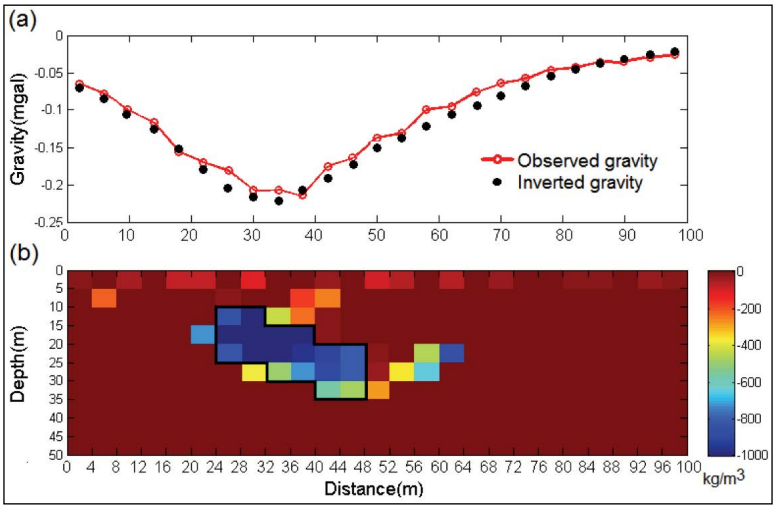

Figure 7- a) Observed gravity due to model in figure 3(b) as corrupted with 15% noise and inverted gravity due to b) inverted model. the initial assumed model outlined with black line.

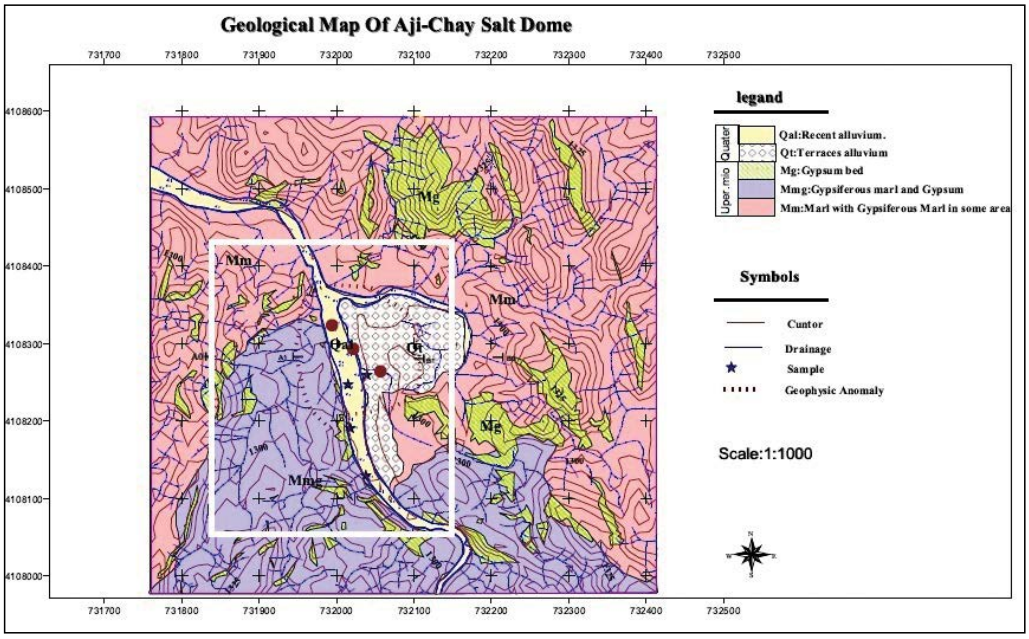

Figure 8- The geological map of area under investigation.

are our desire, are appeared (Figure 12). Because of the less density of the salt dome than around domain, it is recognizable on the residual gravity anomalies map with negative anomaly.

From negative anomaly due to the salt dome was sampled at 17 points with about 11.3 m interval along profile *AB*. Profile *AB* in anomaly is specified in E-W direction, which is shown in figure 12.

The variation of the gravity field along profile AB is shown in figure 13 (a). For inverting the observed gravity, we divided the inversion domain into 33×21 blocks of dimension 5.8 m in the x direction and 5 m in the y direction. Therefore, the whole domain is 192 m × 105 m, i.e. 20160 m^2. The ε and initial l_0 values were specified as 10^{-12} and near to zero respectively. We have also considered the average density of the salt dome about 2200 kg/m^3. Considering the geological formation, sediments and layer material

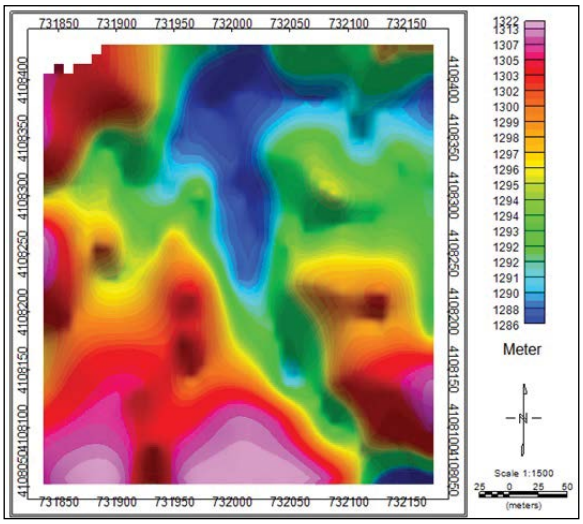

Figure 9- The topography map of the region under gravity survey.

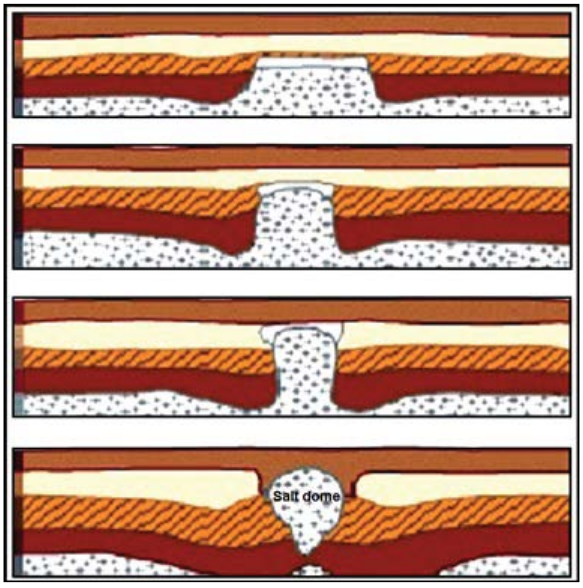

Figure 10- The process of salt dome formation in the region of the northwest of Iran.

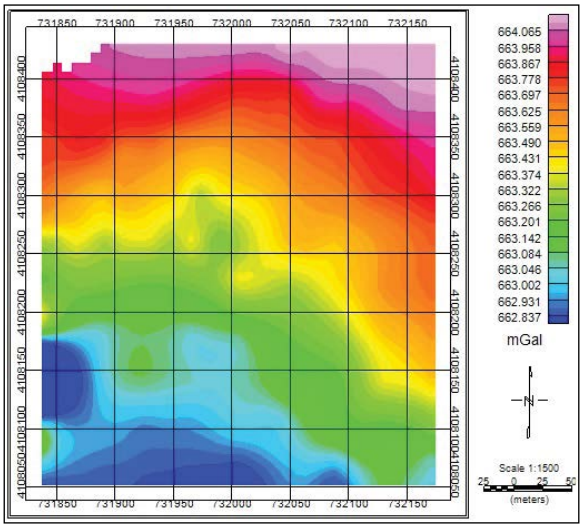

Figure 11- The Bouguer gravity anomaly map of the area under evaluation.

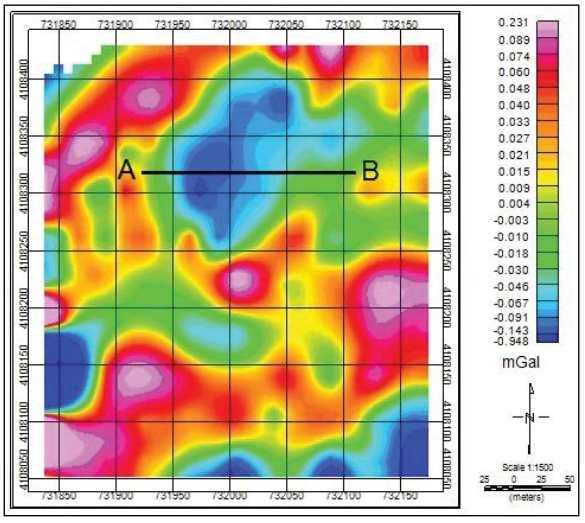

Figure 12- The residual gravity anomalies map of the area under evaluation. The position of the profile AB over the negative gravity anomaly due to the salt dome has been specified.

of the area under investigation, the average density of subsurface domain is given as 2500 kg/m^3. Then, the density contrast was taken to be -300 kg/m^3. Figure 13 (b) display the distribution of the inverted density after 18 iterations. The estimated L1 norm for each iteration is shown in figure 14. The L1 norm lessen from the its initial value of 1.576 mGal at the first iteration to 0.162 mGal at the 18th iteration

The inverted gravity produced by the determined densities for juxtaposed prisms is shown in figure 13 (a). The density distribution demonstrate the geometry of the salt dome whose main concentration is at a depth of 42 m and a horizontal distance of 60 m from the profile AB origin, where the density contrast is about -300 kg/m^3. By getting away from the center of salt dome in all directions, because of admixing the salt with sediment and alluvial material the density contrast amount diminish. The simulated salt dome show a elongation in the diffusion of the density towards east (right). If we consider the density contrast of -200 kg/m^3 as the salt dome limited area, therefore it have a depth to top of about 27 m and a depth to bottom of about 65 m.

For comparison, we have used from ModelVision software in order to nonlinear inverse modeling of the measured gravity data due to the salt dome. The gravity sampling was accomplish at 33 points with 10 m interval along the profile A′B′ which depicted on the gravity anomaly of the salt dome, as is shown in figure 15(a). The variation of the gravity field along profile A′B′ is shown in the upper part of figure 15(b) (black line). We have considered a spherical initial model situated on the profile A′B′ whose the location of horizontal and vertical cross-section (violet circle) has been presented in figure 15(a) and the down part of the figure 15(b), respectively. The blue line in the upper part of figure 15(b) indicate the gravity anomaly caused by the assumed model.

The software tries to minimize the error between the observed gravity and inverted gravity (the upper part of figure 16 b) by changing the model parameters, i.e. the depth to top and bottom and radiuses in three directions. The horizontal and vertical cross-section of the final model are displayed through figure 16(a) and the down part of the figure 16(b). The estimated upper and lower surfaces depth of inferred model are about 25 m and 73 m, respectively and the maximum horizontal extension is about 70 m.

6. Conclusions

In this paper, a compact inversion method based on introduced approach by Last and Kubik (1983) is employed. For increasing the depth resolution and eluding the tendency of placement the structure too close to the surface is used a depth weighting function in the inversion algorithm. The convergence and consistency of the proposed method was evaluated with two synthetic gravity data, with and without random noise, due to two theoretical models. The L1

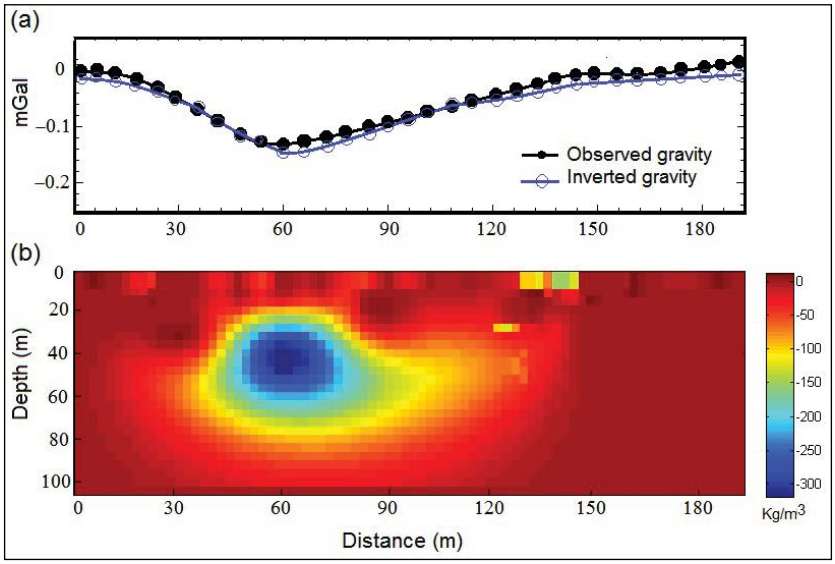

Figure 13- a) Observer gravity along profile AB and inverted gravity due to b) inverted structure.

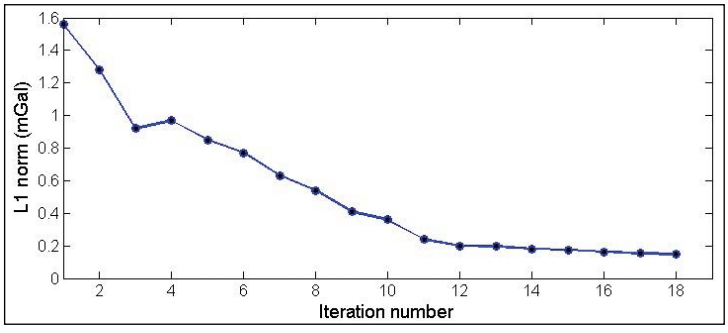

Figure 14- Variations L1 norm values versus iteration number during inversion of the real gravity data.

norm was considered as the stopping criterion of the iteration. The inverted density from interpretation the synthetic data are completely similar to the assumed models. We have inverted a real 2D gravity data set due to a salt dome using the linear inversion method. Usually for low N/S values a satisfying convergence of the solution is obtained. For real gravity data, we have considered a near to zero value for l_o until the noise was interpreted geologically, in other words, noise-weighting matrix be determined based on the estimated density in the each iteration.

The inverted density has been distributed smoothly overall the inversion domain where the centralization of the high density contrast (about -300 kg/m^3) indicate the core of salt dome. The modeled domain shows that with increasing distance from the core of salt dome, the density contrast dwindle, therefore the interface between salt deposit and surroundings is not a sharp and distinct border.

We also analyzed the real gravity data using the ModelVision software. The inferred structure from nonlinear inversion, i.e. ModelVision software, show good conformity with inverted structure from linear inversion, i.e. proposed method. With respect to the results can infer that the described inversion technique is a powerful and practicable instrument for interpreting the gravity field.

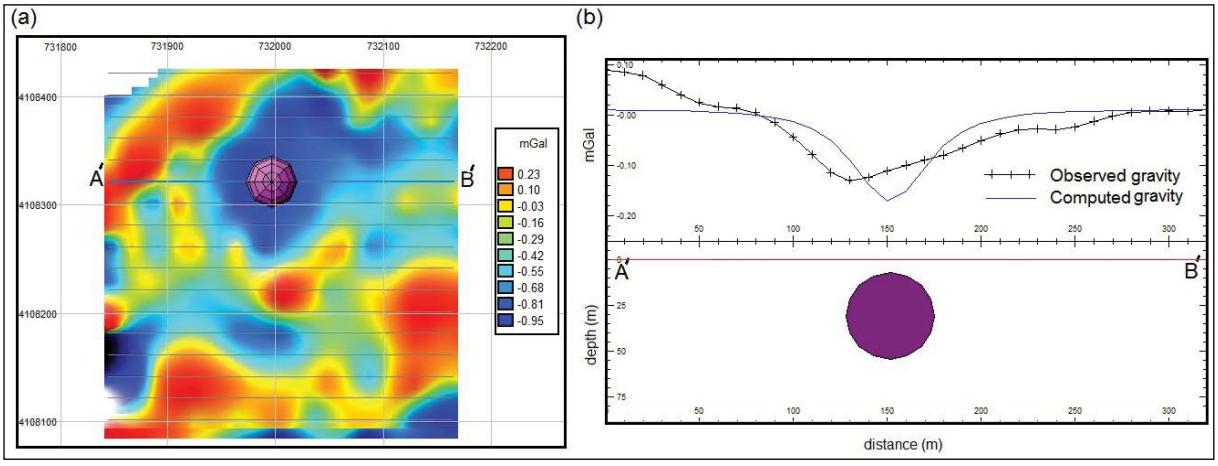

Figure 15- a) The horizontal cross-section of the initial model situated on the gravity anomaly of the salt dome where the profile A′B′ go across. b) gravity field changes through the profile A′B′ (black line) and calculated gravity (blue line) due to the initial model as the vertical cross-section of it has been displayed.

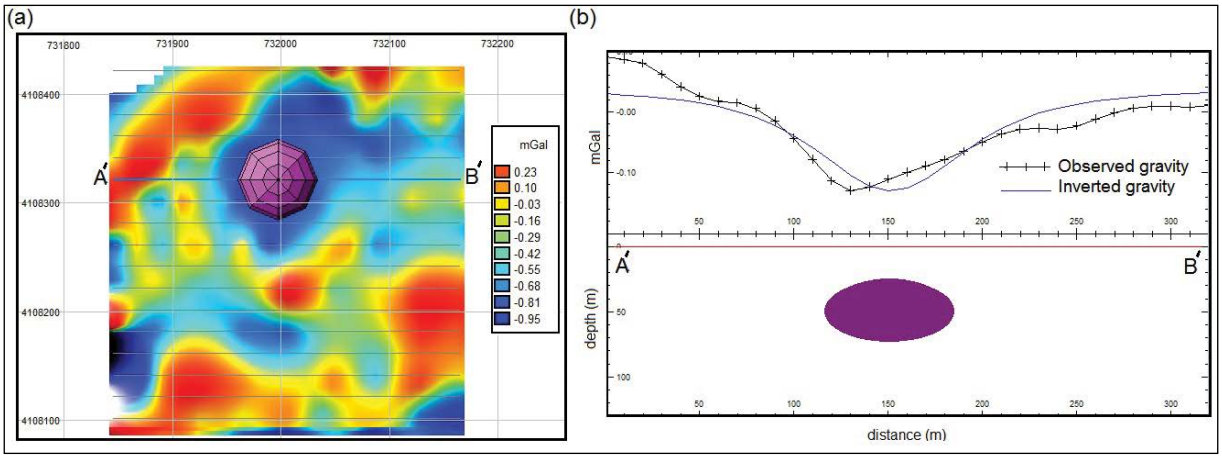

Figure 16- a) Horizontal cross- section of the final inferred model using the nonlinear inversion of gravity data of the profile A′B′. b) The inverted gravity produced by the resulted structure (blue line). The vertical cross-section of the final inversion model has been shown in the down part of the Figure 15(b).

References

Abdelrahman, E.M. 1990. Discussion on "A least-squares approach to depth determination from gravity data" by O. P. Gupta. Geophysics, 55, 376-378.

Abdelrahman, E.M., El-Araby, T.M. 1993. A least-squares minimization approach to depth determination from moving average residual gravity anomalies. Geophysics, 58,1779–1784.

Abdelrahman, E.M., El-Araby, H.M. 1993. Shape and depth solutions from gravity using correlation factors between successive least-squares residuals. Geophysics, 59, 1785–1791.

Abdelrahman, E.M., Bayoumi, A.I., Abdelhady, Y.E., Gobashy, M.M., El-Araby, H.M. 1989. Gravity interpretation using correlation factors between successive least-squares residual anomalies. Geophysics, 54, 1614-1621.

Abdelrahman, E.M., Bayoumi, A.I., El-Araby, H.M. 1991. A least-squares minimization approach to invert gravity data. Geophysics, 56, 115-l 18.

Al-Garni, M.A. 2013. Inversion of residual gravity anomalies using neural network. Arab J Geosci, 6,1509–1516.

Asfahani, J., Tlas, M. 2008. An automatic method of direct interpretation of residual gravity anomaly profiles due to spheres and cylinders. Pure and Applied Geophysics, 165/5, 981–994.

Biswas, A. 2015. Interpretation of residual gravity anomaly caused by a simple shaped body using very fast simulated annealing global optimization. Geoscience Frontiers, 6/6, 875–893.

Biswas, A. 2016. Interpretation of gravity and magnetic anomaly over thin sheet-type structure using very fast simulated annealing global optimization technique. Modeling Earth Systems and Environment, 2/1, 30.

Biswas, A. 2018. Inversion of source parameters from magnetic anomalies for mineral /ore deposits exploration using global optimization technique and analysis of uncertainty. Natural Resources Research, 27/1, 778–107.

Biswas, A., Sharma, S. P. 2016. Integrated geophysical studies to elicit the structure associated with Uranium mineralization around South Purulia Shear Zone, India: A Review. Ore Geology Reviews, 72, 1307–1326.

Biswas, A., Mandal, A., Sharma, S. P., Mohanty, W. K. 2014*a*. Delineation of subsurface structure using self-potential, gravity and resistivity surveys from South Purulia Shear Zone, India: Implication to uranium mineralization. Interpretation, 2/2, T103–T110.

Biswas, A., Mandal, A., Sharma, S. P., Mohanty, W. K. 2014*b*. Integrating apparent conductance in resistivity sounding to constrain 2D Gravity modeling for subsurface structure associated with uranium mineralization across South Purulia Shear Zone. International Journal of Geophysics, Article ID 691521, 1–8.

Biswas, A., Parija, M. P., Kumar, S. 2017. Global nonlinear optimization for the interpretation of source parameters from total gradient of gravity and magnetic anomalies caused by thin dyke. Annals of Geophysics, 60/2, G0218, 1–17.

Bosch, M., McGaughey, J. 2001. Joint inversion of gravity and magnetic data under lithological constraints. The Leading Edge, 20, 877–881.

Bosch, M., Meza, R., Jiménez, R., Hönig, A. 2006. Joint gravity and magnetic inversion in 3D using Monte Carlo methods: Geophysics, 71/4, G153–G156.

Bowin, C., Scheer, E., Smith, W. 1986. Depth estimates from ratios of gravity, geoid, and gravity gradient anomalies. Geophysics, 51, 123-136.

Chakravarthi, V., Sundararajan, N. 2004. Ridge regression algorithm for gravity inversion of fault structures with variable density. Geophysics, 69, 1394–1404.

Eshaghzadeh, A., Kalantary, R.A. 2015. Anticlinal Structure Modeling with Feed Forward Neural Networks for Residual Gravity Anomaly Profile, 8th congress of the Balkan Geophysical Society, DOI: 10.3997/2214-4609.201414210.

Eshaghzadeh, A., Hajian, A. 2018. 2-D inverse modeling of residual gravity anomalies from Simple geometric shapes using Modular Feed-forward Neural Network, Annals of Geophysics. 61,1, SE115.

Essa, K.S. 2007. A simple formula for shape and depth determination from residual gravity anomalies. Acta Geophysica, 55/2, 182–190.

Farquharson, C. G., Ash, M. R., Miller, H. G. 2008. Geologically constrained gravity inversion for the Voisey's Bay ovoid deposit. The Leading Edge, 27, 64–69.

Gallardo, L. A., Meju, M. 2003. Characterization of heterogeneous near-surface materials by joint 2D inversion of DC and seismic data: Geophysical Research Letters, 30, L1658.

Ganguli, S.S., Dimri, V. P. 2013. Interpretation of gravity data using eigen image with Indian case study: A SVD approach. Journal of Applied Geophysics, 95, 23-35.

Ganguli, S.S., Lashin, A.A., Al Arifi, N.S., Dimri, V. P. 2015. Design of Gravity energy filter to enhance signal-to-noise ratio of gravity measurements. Jour. of Ind. Geophy. Union, 19/3, 333-338.

Gupta, O.P. 1983. A least-squares approach to depth determination from gravity data. Geophysics, 48, 357-360.

Hammer, S. 1977. Graticule spacing versus depth discrimination in gravity interpretation. Geophysics, 42, 60-65.

Heincke, B., Jegen, M., Moorkamp, M., Chen, J., Hobbs, R.W. 2010. Adaptive coupling strategy for simultaneous joint inversions that use petrophysical information as constraints: 80th Annual International Meeting, SEG, Expanded Abstracts, 29, 2805–2809.

Ialongo, S., Fedi, M., Florio, G. 2014. Invariant models in the inversion of gravity and magnetic fields and their derivatives. Journal of Applied Geophysics, 110, 51-62.

Kamm, J., Lundin, I.A., Bastani, M., Sadeghi, M., Pedersen, L.B. 2015. Joint inversion of gravity, magnetic, and petrophysical data — A case study from a gabbro intrusion in Boden, Sweden. Geophysics, 80/5, B131–B152.

Last, B. J., Kubik, K. 1983. Compact gravity inversion, Geophysics,48, 713-721.

Lelièvre, P.G., Farquharson, C.G., Hurich, C.A. 2012. Joint inversion of seismic traveltimes and gravity data on unstructured grids with application to mineral exploration. Geophysics, 77, K1–K15.

Li, Y., Oldenburg, D. W. 1998. 3-D inversion of gravity data. Geophysics, 63, 109-119.

Lines, L.R., Treitel, S. 1984. A review of least-squares inversion and its application to geophysical problems. Geophys. Prosp, 32, 159-186.

Mandal, A., Biswas, A., Mittal, S., Mohanty, W. K., Sharma, S. P. Sengupta, D., Sen, J., Bhatt, A. K. 2013. Geophysical anomalies associated with uranium mineralization from Beldih mine, South Purulia Shear Zone, India. Journal Geological Society of India, 82/6, 601–606.

Mandal, A., Mohanty, W. K., Sharma, S. P., Biswas, A., Sen, J., Bhatt, A. K. 2015. Geophysical signatures of uranium mineralization and its subsurface validation at Beldih, Purulia District, West Bengal, India: A case study. Geophysical Prospecting, 63, 713–726.

Menke, W. 2012. Geophysical Data Analysis: Discrete inverse theory (MATLAB Edition), Elsevier Inc., New York, 293 s.

Mohan, N.L., Anandababu, L., Rao, S. 1986. Gravity interpretation using the Melin transform, Geophysics. 51, 114-122.

Odegard, M.E., Berg, J.W. 1965. Gravity interpretation using the Fourier integral. Geophysics, 30, 424-438.

Oldenburg, D. W. 1974. The inversion and interpretation of gravity anomalies. Geophysics, 39/4, 526-536.

Osman, O., Muhittin, A.A., Uçan, O.N. 2006. A new approach for residual gravity anomaly profile interpretations: Forced Neural Network (FNN). Ann. Geofis, 49, 6.

Osman, O., Muhittin, A.A., Uçan, O.N. 2007. Forward modeling with Forced Neural Networks for gravity anomaly profile. Math. Geol, 39, 593-605.

Parker, R. L. 1973. The Rapid Calculation of Potential Anomalies. Geophysical Journal of the Royal Astronomical Society, 31, 447-455.

Pilkington, M. 2006. Joint inversion of gravity and magnetic data for twolayer models. Geophysics, 71/3, L35–L42.

Salem, A., Ravat, D., Johnson, R., Ushijima, K. 2001. Detection of buried steel drums from magnetic anomaly data using a supervised neural network. J. Environ. Eng. Geophys, 6,115-122.

Saxov, S., Nygaard, K.1953. Residual anomalies and depth estimation. Geophysics, 18, 913-928.

Shamsipour, P., Marcotte, D., Chouteau, M., Keating, P. 2010. 3D stochastic inversion of gravity data using cokriging and cosimulation. Geophysics 75, I1–I10.

Shamsipour, P., Chouteau, M., Marcotte, D. 2011. 3D stochastic inversion of magnetic data. Journal of Applied Geophysics 73, 336–347.

Shamsipour, P., Marcotte, D., Chouteau, M. 2012. 3D stochastic joint inversion of gravity and magnetic data. Journal of Applied Geophysics 79, 27–37.

Sharma, B., Geldart, L.P. 1968. Analysis of gravity anomalies of two-dimensional faults using Fourier transforms. Geophys. Prosp, 77-93.

Shaw, R. K., Agarwal, N.P. 1990. The application of Walsh transforms to interpret gravity anomalies due to some simple geometrically shaped causative sources: A feasibility study. Geophysics, 55, 843-850.

Singh, A., Biswas, A. 2016. Application of global particle swarm optimization for inversion of residual gravity anomalies over geological bodies with idealized geometries. Natural Resources Research, 25/3, 297–314.

Skeels, D. C. 1947. Ambiguity in gravity interpretation, Geophysics, 12, 43-56.

Srivastava, R.P., Vedanti, N., Dimri, V.P. 2007. Optimal Design of a Gravity Survey Network and its Application to Delineate the Jabera-Damoh Structure in the Vindhyan Basin, Central India. Pure & App. Geophy, 164/10, 2009-2022.

Tschirhart, V., Morris, W. A., Jefferson, C.W., Keating, P., White, J. C., Calhoun, L. 2013. 3D geophysical inversions of the north-east Amer Belt and their relationship to the geologic structure. Geophysical Prospecting, 61, 547–560.

Tschirhart, V., Jefferson, C.W., Morris, W.A. 2017. Basement geology beneath the northeast Thelon Basin, Nunavut: insights from integrating new gravity, magnetic and geological data. Geophysical Prospecting, 65, 617-636.

Tsuboi, C. 1983. Gravity, 1st edn. George Allen ve Unwin Ltd, London, 254 pp.

Williams, N. C. 2008. Geologically-constrained UBC-GIF gravity and magnetic inversions with examples from the Agnew-Wiluna Greenstone Belt, Western Australia: Ph.D. thesis, University of British Colombia.

Zeyen, H., Pous, H. 1993. 3-D joint inversion of magnetic and gravimetric data with a priori information. Geophysical Journal International, 112, 244–256.